(γ,np) reactions in ^{12}C, ^{6}Li and $^{3,4}He$

S.N. Dancer, I.J.D. MacGregor, J.R.M. Annand, I. Anthony, G.I. Crawford, S. Doran, S.J. Hall, J.D. Kellie, J.C. McGeorge, R.O. Owens, P.A. Wallace (Glasgow), D. Branford, S.V. Springham, A.C. Shotter (Edinburgh), R. Beck, R. Gothe, F. Kalleicher, G. Liesenfeld, H. Schmieden, B. Schoch, J. Vogt, F. Zettl (Mainz), S. Klein (Tubingen).

The emission of neutron-proton pairs is the most probable outcome of photon absorbtion in the energy region above the giant resonance at least up to the pion threshold, but little detailed information on the process has been obtained due to experimental difficulties. Two nucleon emission following photon absorbtion by a correlated pair is favoured compared to direct knockout of a single nucleon, which is suppressed by the large momentum mismatch between the ingoing photon and a single outgoing fast nucleon. Studies of the (γ,np) process seek firstly to obtain a quantitative understanding of the photon interaction mechanism, and through this to open the door to investigations of nucleon correlations in nuclei [1], information about which is long sought but not readily obtainable.

In [1] Gottfried has shown that the (γ,np) cross-section can be parameterised as a product of two factors, one being the distribution of initial momenta of the n-p pair, F(P), and the other dependent on the nucleon-nucleon correlations. However, before one can try to extract information on nucleon correlations, it is essential to establish a quantitative understanding of the reaction mechanism.

In this investigation of the (γ,np) reaction experiments were carried out over as wide a range of nuclear targets and kinematic conditions as was possible. Four light nuclei, ^{12}C, ^{6}Li, ^{4}He and ^{3}He were studied. The nucleons ejected from these targets come from both the 1s and the 1p shells, and from nuclei with significantly different densities. Final state interactions should be small enough so as not to produce serious complications in the analysis for any such light nuclei. The kinematics of the (γ,np) process ensures that the momentum transferred between the

correlated nucleons depends most strongly on the photon energy. For this reason, the experiments sought to cover as wide a range of photon energies as possible, at the expense of not covering the full angular range at each energy.

Most (γ,np) experiments [2-5] have used Bremsstrahlung beams and have not defined the energies of the incident photon and emerging nucleons well enough to allow an accurate kinematic reconstruction of each event. In many cases only the angular correlation between the nucleons was examined and this is sensitive principally to the low momentum part of the initial shell model wavefunctions. Very little information was obtained on the overall strength of the (γ,np) process and its dependence on photon energy and the shells from which the nucleons are ejected. More recently some higher energy studies [6,7] (200-400 MeV) have been carried out using tagged photons. However the best overall energy resolution obtained, ~30 MeV, was still insufficient to give useful information on the initial shells of the emitted nucleons.

The present measurements considerably alleviate the previous experimental difficulties by making use of the 100% duty cycle electron beam from the MAMI-A microtron in conjunction with the GEM tagged photon spectrometer [8]. Fig. 2.1 shows a schematic diagram of the set-up. Two settings of the tagging system were used to cover the photon energy ranges 83-133 MeV and 133-158 MeV. Protons, and other charged particles, were detected in a large solid angle scintillator telescope [9]. This has an energy resolution of 2.8 MeV (at 60 MeV), an angular resolution of 3° and a useful solid angle of 0.7 sr. This detector was placed at 90° to the incident photon beam and detected charged particles in the angular range 45° to 135°. Neutrons were detected by an array of plastic scintillator time-of-flight spectrometers. The initial runs made use of 8 20x20x100 cm^3 neutron detectors which had an energy resolution of ~6 MeV (at 50 MeV) and subtended a solid angle of ~0.10 sr when placed 4 m from the target. In later runs these were supplemented by 24 additional 10x20x180 cm^3 detectors [10] which were placed 3 m from the target giving a 5x improvement in overall data rate. The energy resolution of these new detectors was ~4.5 MeV (at 50 MeV). For most of the later measurements

a ΔE scintillation detector was placed on the neutron detector side of the target to distinguish (γ,pp) and (γ,pd) events from (γ,pn) events.

The ^{12}C data were taken using thin graphite and CD_2 targets. The CD_2 target also provided a normalisation to the $d(\gamma,p)n$ reaction and an energy calibration of the proton detector.

The ^{6}Li target was sealed with thin air-tight foils. The target thickness was determined to ~2% by comparing pair production from it and a standard target. The energy straggling (~10 MeV) produced by the thick target used was not a problem in the case of ^{6}Li, as ~20 MeV is required to remove a nucleon from the 1s shell, and it was still possible to separate those events which left the residual α-particle intact from those which did not.

Cryogenic target systems were constructed for both ^{4}He and ^{3}He. For ^{4}He a simple system was made from a commercial dewar-type cryostat. Although heat losses were reduced by using a liquid nitrogen cooled interstage and heat shield, it was found necessary to replenish the helium every 3 hours. For ^{3}He it was necessary to build a more complicated system in which liquefaction is achieved by pumping the helium around a closed loop containing a Joule-Kelvin expansion valve. This system permitted the ^{3}He to be recovered to a buffer for subsequent re-use. The ~1 cm thick target cell was fitted with 70μm thick kapton windows and housed in a 9 cm radius cylindrical vacuum chamber. This chamber had 120μm thick kapton windows for entrance and exit of the photon beam and for exit of hadronic reaction products. The two arm particle detection system described above was used with the addition of two curved 1 mm thick scintillators which fitted closely round the vacuum chamber housing the target. These formed the front element of the E,ΔE telescope and acted as particle identifier in the time-of-flight spectrometer.

The data were recorded and analysed event by event. Off-line processing [11,12] allowed rejection of background, selection of prompt coincidences and correction for randoms and neutron detector efficiencies.

$^{12}C(\gamma,np)$

Two measurements of the $^{12}C(\gamma,np)$ reaction were carried out, one in 1985 and the other in 1986. The first measurement covered the energy range 83 to 133 MeV while the second for which the improved neutron TOF detectors were available covered the energy range 83-158 MeV. The results shown here are from the analysis of the first data. The later data is still being analysed. Fig. 3.1 shows the $^{12}C(\gamma,np)$ missing energy spectrum for photon energies between 113 and 133 MeV. For the first time in a $^{12}C(\gamma,np)$ experiment the resolution is sufficient to provide useful information on the shells from which the nucleons have been ejected. However the data do not exhibit structure which would allow a totally unambiguous separation of events in which two 1p nucleons are emitted, from those in which a more tightly bound 1s shell nucleon is ejected. Nevertheless the peak centred at $E_m \simeq 28$ MeV, close to the $^{12}C(\gamma,pn)$ reaction threshold (27.4 MeV), has a width little greater than the overall resolution and indicates a large probability of leaving the residual ^{10}B in its ground or low lying states. For the purpose of further analysis events with $15\ \text{MeV} < E_m < 40\ \text{MeV}$ were assumed to result from the emission of two 1p nucleons. Fig. 3.2 shows the observed distribution of initial momentum P of the participating neutron-proton pair for these events. Also shown (solid line) is the result of a calculation using Saxon-Woods wavefunctions after correction for the finite angular and energy acceptance of the detectors. This shows very good agreement with the data. Comparison was also made with the distribution expected if the final state kinematics were determined purely by phase space considerations (dashed line), again after correction for the detector acceptances. The difference from the quasideuteron prediction is distinct. A similar conclusion results from consideration of the three components of $\underline{P}$. As an example the distribution of the component along the beam axis is shown in fig. 3.3. The peak in the deuterium data centered near zero confirms the correct calibration of the detector system and gives an indication of the resolution. Figs. 3.2 and 3.3 provide persuasive evidence that the quasideuteron description is quantitatively correct. The distinction between quasideuteron and phase space predictions should be larger in higher E_γ data still to be analysed.

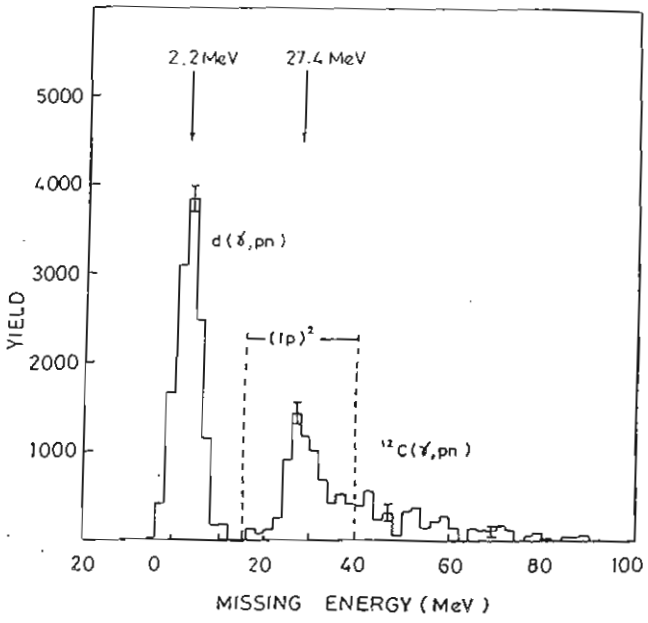

Fig. 3.1 Missing energy spectrum for $113<E_\gamma<133$ MeV observed with a CD_2 target.

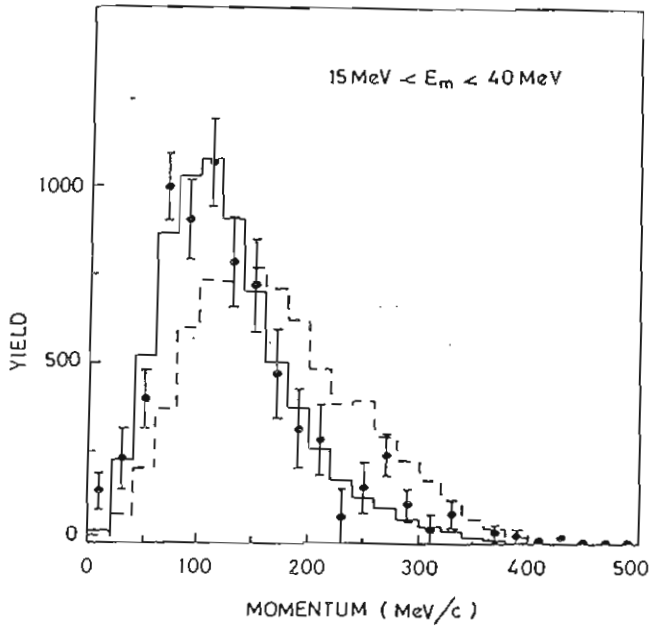

Fig. 3.2 Initial momentum distribution of the n-p pair observed in the $^{12}C(\gamma,np)$ reaction for $113<E_\gamma<133$ MeV when both nucleons are emitted from the p-shell. The solid line results from a calculation using Saxon-Woods wavefunctions while the dashed line represents the results of a phase space calculation.

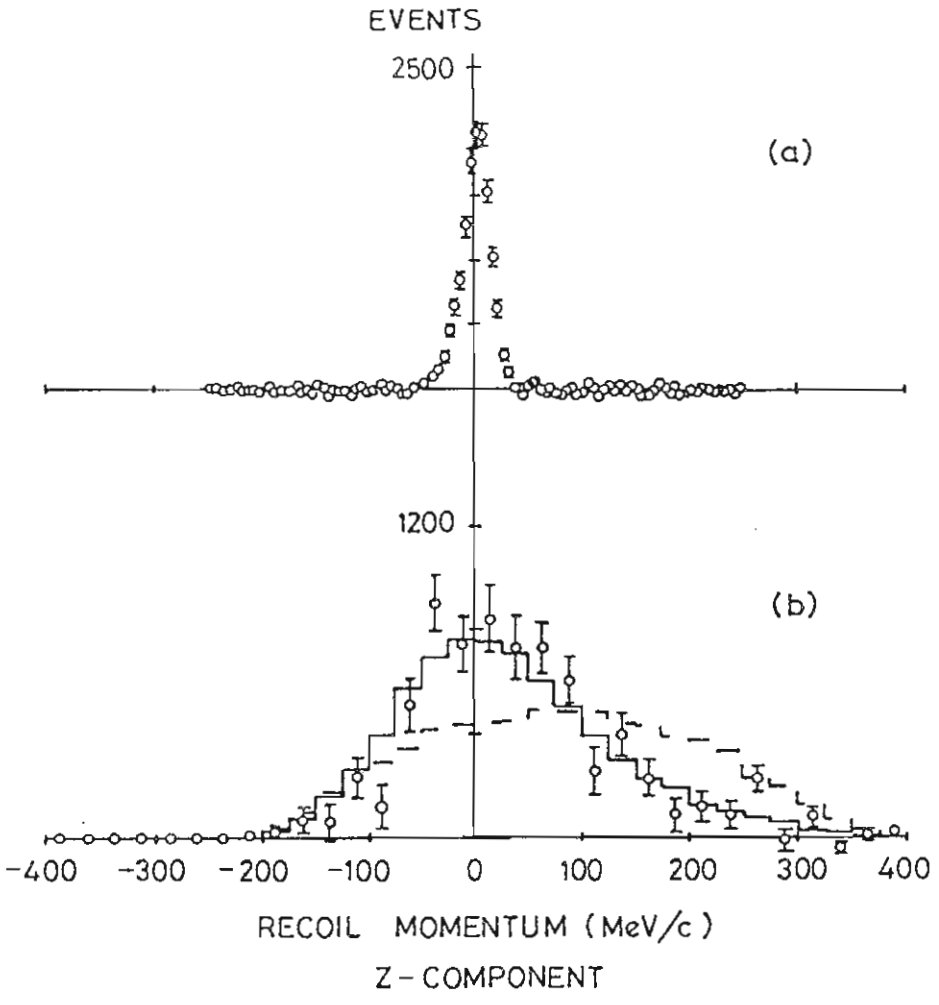

Fig. 3.3 Distribution of the initial n-p pair momentum component along the photon beam direction observed in
a) Deuterium data, b) Carbon $(1p)^2$ data.
The lines have the same meaning as in fig. 3.2.

In the quasideuteron model [13] the strength of the photon absorption cross section is parameterised by the Levinger parameter L determined by the relative probability of closely spaced nucleon pairs in the target nucleus compared to the deuteron. A value of ~6 is expected for ^{12}C. The present data yield an uncorrected value of 3.9 for events in which both nucleons are ejected from the 1p shell. A reduction of this order is expected due to the effects of final state interactions (FSI) which scatter or absorb the outgoing nucleons. Events in which the encounter

is highly inelastic will have a missing energy larger than the range included in this analysis and will be lost as noted above. More nearly elastic scattering of an outgoing nucleon will lead to the deduced initial pair momentum being incorrect. Such events will have an F(P) distribution closer to the phase space prediction. However in fig. 3.2 there is little sign of a significant excess over the quasideuteron prediction at higher momenta which suggests that this process is of lesser importance.

In later data at E_γ = 83-133 MeV many more events were recorded. This will give much improved statistical accuracy in figs. 3.1, 3.2 and 3.3. Data has also been taken recently at E_γ = 133-158 MeV which will extend the missing energy spectrum to higher E_m values.

^{6}Li(γ,np)

The (γ,np) reaction on ^{6}Li in the low missing energy region has a particularly simple interpretation, as the two 1p nucleons in ^{6}Li are very loosely bound. Interactions with these "valence" nucleons simply strip the α-particle core, leaving it intact. A comparison with the d(γ,np) cross-section is particularly interesting as the deuteron and the two outer nucleons in ^{6}Li have similar sizes and separation energies. More inelastic interactions involving the 1s nucleons lead to the break-up of the α-core. It will be of interest to compare this process with the ^{4}He(γ,np) reaction, i.e. the breakup of the real α particle.

Two measurements of the ^{6}Li(γ,np) reaction were carried out in 1985. The first measurement covered the tagged photon energy range 83 to 133 MeV while the second measurement covered the higher energy range 133 to 158 MeV. Fig. 3.4 shows the ^{6}Li missing energy spectrum for the first data. The poorer resolution (cf. fig. 3.1) is due to the thicker target used and the fact that the neutron detectors were placed 2 m from the target to increase the solid angle in this experiment. It is nevertheless possible to separate those events in which the residual α-particle remains intact from those in which it does not. The discussion

concentrates on the lower missing energy data as the higher missing energy region has not yet been fully analysed.

Fig. 3.5 shows a 2-dimensional plot of recoil kinetic energy vs missing energy. The recoil α-particles are seen to have little kinetic energy, consistent with the fact that the emitted particles are weakly bound. The recoil momentum distribution, F(P), is shown in fig. 3.6 on a logarithmic scale. Also shown (solid line) is the quasideuteron prediction using Harmonic Oscillator nucleon wavefunctions with an oscillator parameter fitted to the low momentum region. The agreement is good in the fitted region, but at higher momenta the data show no evidence of the strong minimum predicted by the model. Calculations are currently being carried out to see whether better agreement might be obtained using Woods-Saxon wavefunctions.

Normalisation of the (γ,np) cross-section to the $D(\gamma,p)$ cross-section is both easy and very reliable in case of ^{6}Li since the Q value of the (γ,np) reaction in ^{6}Li is close to that of deuteron. The ratio of the quasideuteron cross-section to the deuterium cross-section is shown in fig. 3.7 for the low missing energy peak in ^{6}Li. The data are seen to be consistent with the low energy bremsstrahlung data of Wade et al. [14] and the $^6Li(\pi^+,pp)\alpha$ data of Bressani et al. [15]. The solid line is a fit to the Levinger formula with damping factor

$$\sigma_{QD} = \frac{NZ}{A} L \sigma_D e^{-D/E_\gamma}$$

where σ_D is the deuteron cross-section. The fit gives values of L = 8.4 and D = 82 MeV. It would also be valuable to compare the $Li(\gamma,np)\alpha$ cross-section with the meson exchange part of the deuteron cross-section. It might be expected that this ratio will be independent of E_γ and this interesting question is presently being investigated.

Further data, using the new neutron detectors, was obtained in 1987 and this should improve the resolution and statistics when the analysis is complete. Analysis of the inelastic data is also currently underway.

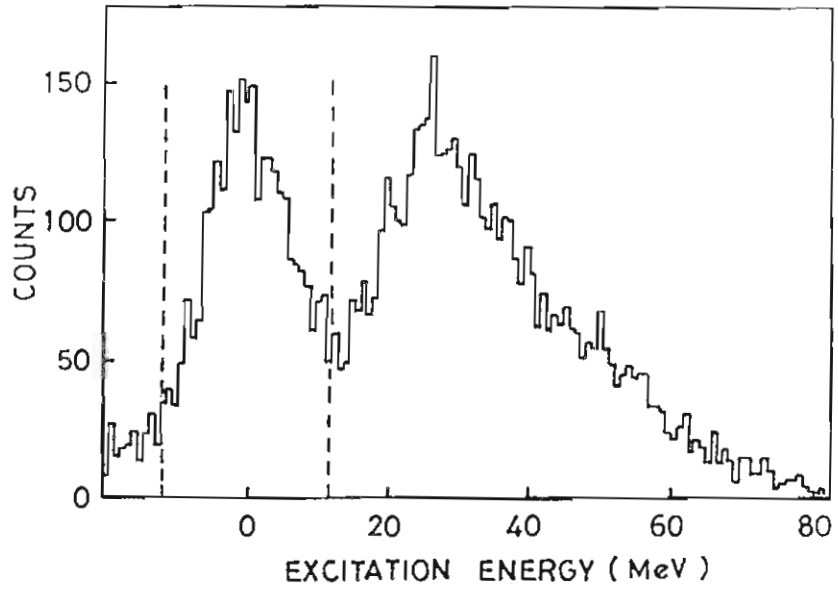

Fig. 3.4 Missing energy spectrum observed in the $^{6}Li(\gamma,p)$ reaction for $80<E_{\gamma}<130$ MeV. For events between the dashed lines the residual α-particle remains intact.

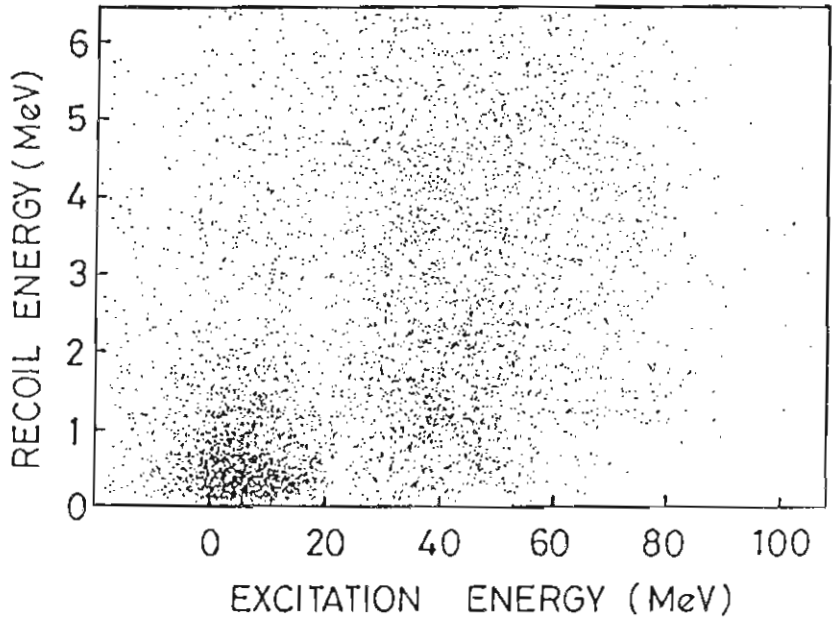

Fig. 3.5 The distribution of residual recoil energies in the $^{6}Li(\gamma,np)$ reaction as a function of residual excitation energy for $80<E_{\gamma}<130$ MeV. For those events in the cluster in the lower left of this diagram, the residual α-particle remains intact.

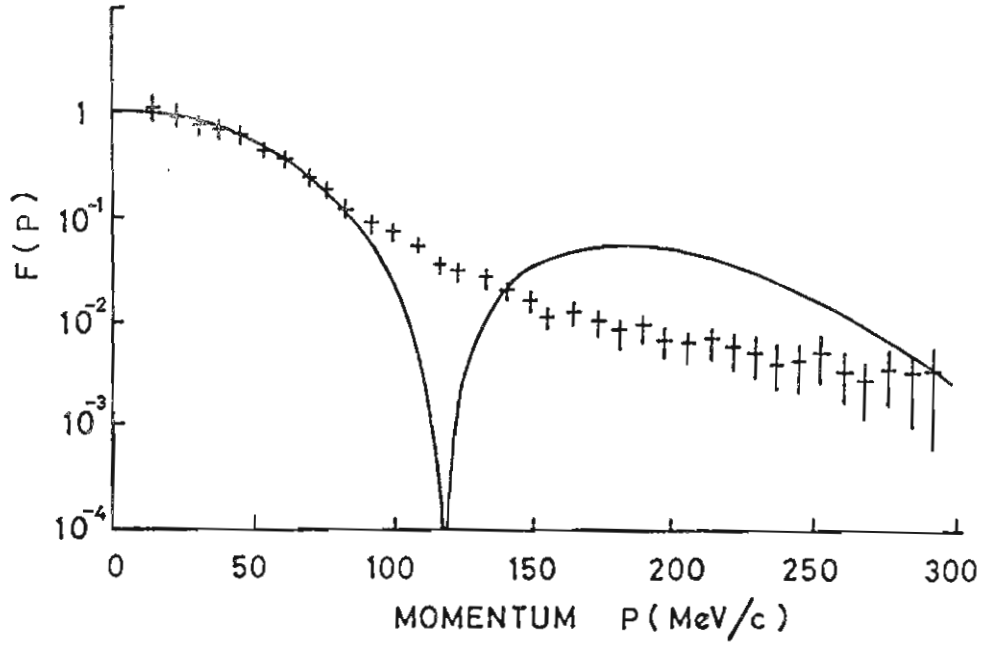

Fig. 3.6 Recoil momentum distribution F(P) observed in the $^{6}Li(\gamma,np)\alpha$ reaction. The solid line represents the result of a calculation using Harmonic Oscillator wavefunctions.

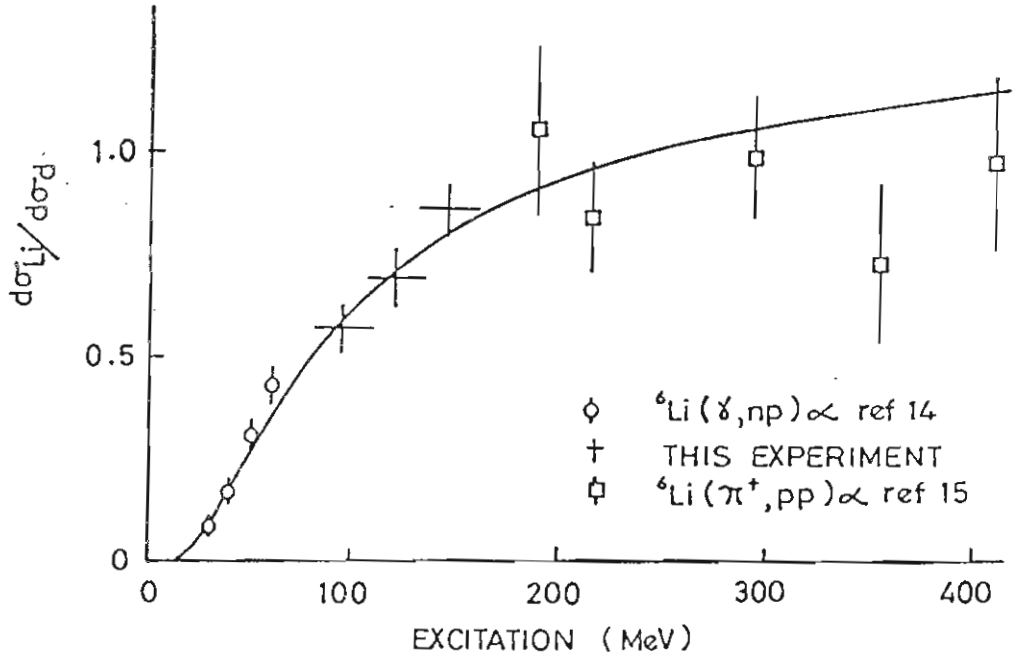

Fig. 3.7

^{3,4}He(γ,np)

The photodisintegration of the helium isotopes should be an especially rewarding study. For example a comparison of the (γ,np) process in ^{3}He and ^{4}He may reveal effects on the N-N correlations due to the differences in the nuclear density. The Helium isotopes have several other breakup modes, for example (γ,pp) and (γ,pd), and these processes have different sensitivities to the various photodisintegration mechanisms. Simultaneous measurement of all of these modes provides a valuable test of the many factors (coupling strengths, form factors etc.) which are used in the theoretical treatment of the photodisintegration process. In ^{3}He complete measurements are possible and the different decay modes will be clearly separated. It is also possible to construct "exact" ^{3}He wavefunctions from any given N-N interaction and to check the calculations with different interactions against the various features of the data. It may for example be possible to find a kinematic region in which the contribution of 3-body forces can be identified.

Two measurements of the photodisintegration of helium in the photon energy range 80-155 MeV were carried out during 1987 and over 100 hours of ^{4}He data were obtained. The analysis is still at an early stage but the performance of the detectors can be judged from fig. 3.8 which shows only a small part (~3 hours) of the data. The E,ΔE plots for the telescope show clearly separated proton and deuteron ridges, while in the TOF spectrometer protons, deuterons and neutrons can be separated, although the low energy response of the neutron detectors is badly compromised by background from the electron beam dump.

The various classes of coincidence event were separated by making cuts on the 2D plots shown in fig. 3.8. The angular distribution of one particle is shown in Fig. 3.9 for coincident events where the angle of the other particle is restricted to a narrow range around 68°. It should be noted that the detection efficiency for charged particles is about 10x that for neutrons. Although (γ,pn) is the most likely process

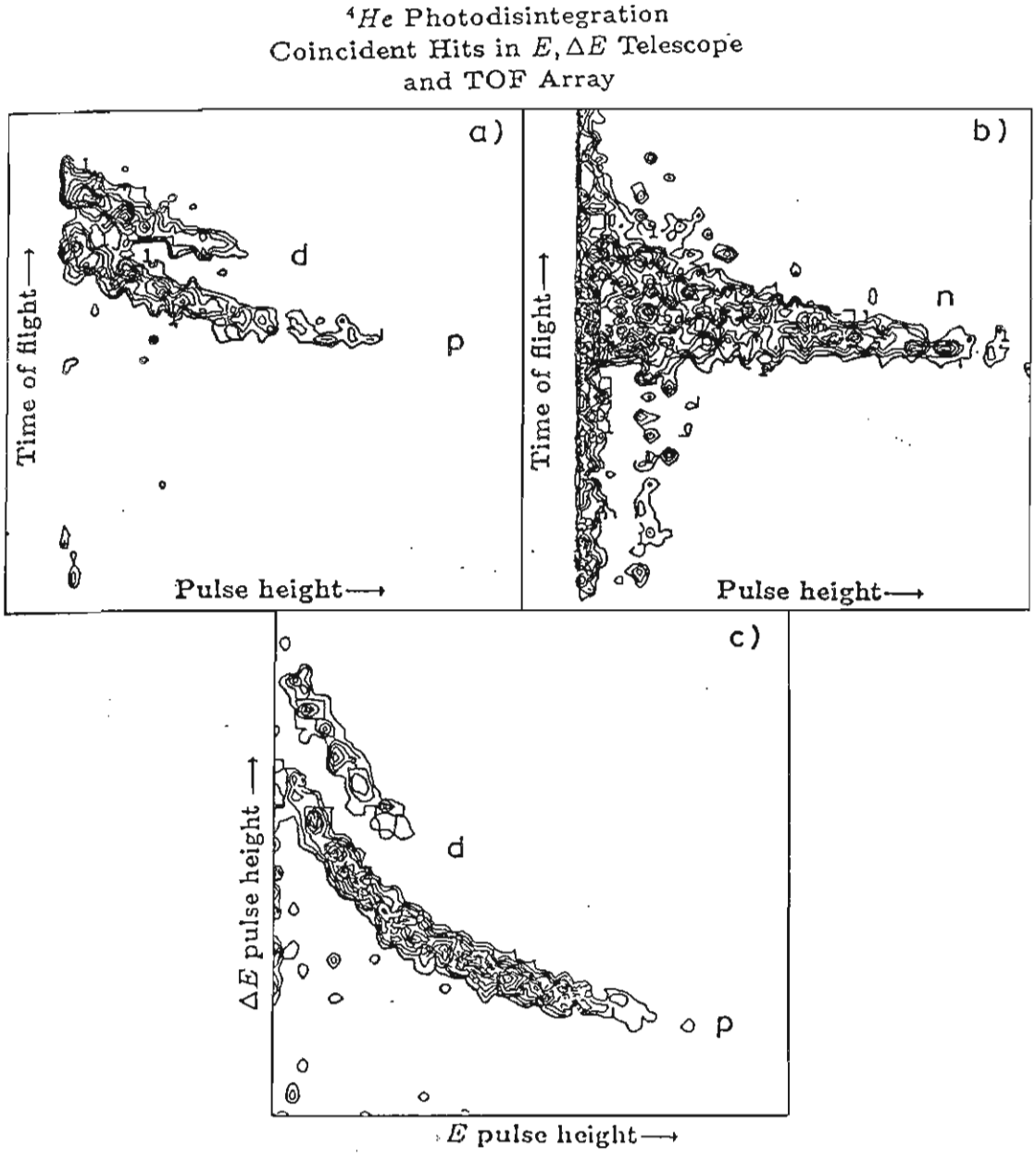

Fig. 3.8 a) TOF/E plot for events which trigger the ΔE counter in the time-of-flight spectrometer.

b) Same for events which do not.

c) ΔE/E plot for the charged particle telescope.

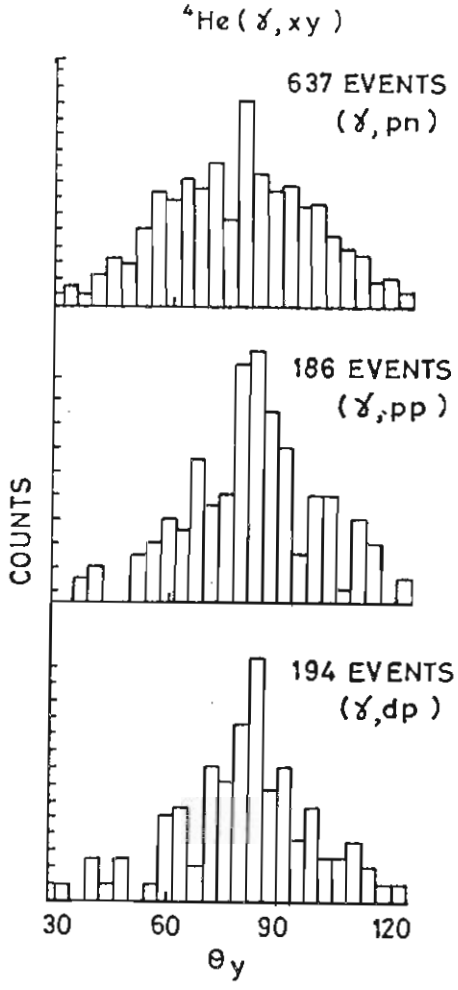

Fig. 3.9 Angular correlations in the ^{4}He(γ,xy) reaction where x is detected at 68±10° to the photon direction.

other particle pairs are also observed. Both the frequency of these other channels and the strong angular correlations observed between the emitted particles are of interest. For example, in the (γ,dp) case it may imply that a "direct" process involving three initial nucleons is involved.

Despite difficulties experienced with the blockages in the expansion valve in the closed loop cryogenic system a small but useful amount of data was also obtained with a ^{3}He target for $130<E_\gamma<155$ MeV. Analysis of all of the data is presently underway.

Conclusions

Evidence from all of the (γ,pn) data studied confirms the dominance of photon absorption on neutron-proton pairs in the intermediate energy region. The present data have an energy resolution which has allowed the shells from which the nucleons are ejected to be identified with reasonable certainty from the missing energy spectra, and an accurate kinematic reconstruction of each event to be carried out. The angular correlation, seen even in early bremsstrahlung experiments, has been measured in much more detail. The distribution of momenta of the initial p-n pairs, has been shown in the case of ^{12}C, to be in quantitative agreement with the prediction of the quasideuteron model. In the case of $^{3,4}He$ the cross sections for competing (γ,pp), (γ,pd) and (γ,dd) reactions have been measured simultaneously and should provide a detailed test of calculations of these reactions.

References

[1] K. Gottfried, Nucl. Phys. 5 (1958) 557.

[2] M.A. Barton and J.H. Smith, Phys. Rev. 110 (1958) 1143.

[3] P.C. Stein et al., Phys. Rev. 119 (1960) 348.

[4] J. Garvey et al., Nucl. Phys. 70 (1965) 241.
I.L. Smith et al., Nucl. Phys. B1 (1967) 483.

[5] H. Hartmann et al., Proc. Asilomar Conference (1973) 967.

[6] S. Homma et al., Phys. Rev. Lett. 52 (1984) 2026.
M. Kanazawa et al., Phys. Rev. C35 (1987) 1828.

[7] J. Ahrends et al., Z. Phys. A298 (1980) 103.

[8] J.D. Kellie et al., Nucl. Instr. and Meth. A241 (1985) 153.

[9] I.J.D. MacGregor et al., Nucl. Instr. and Meth., A262 (1987) 347.

[10] J.R.M. Annand, G.I. Crawford and R.O. Owens, Nucl. Instr. and Meth., 262 (1987) 329.

[11] J.M. Vogt, Dissertation, University of Mainz.

[12] S.N. Dancer, Ph.D. Thesis, University of Glasgow.

[13] J.S. Levinger, Phys. Rev. 84 (1951) 43.

[14] M.V. Wade et al., Phys. Rev. Lett. 53 (1984) 2540.

[15] T. Bressani et al., Nucl. Phys. B9 (1969) 427.